Elastic properties of individual nanometer-size supported gold clusters

D. M. Schaefer
Department of Physics, Purdue University, West Lafayette, Indiana 47907

A. Patil and R.P. Andres
School of Chemical Engineering, Purdue University, West Lafayette, Indiana 47907

R. Reifenberger
Department of Physics, Purdue University, West Lafayette, Indiana 47907
(Received 28 February 1994; revised manuscript received 26 August 1994)

An atomic force microscope has been used in the attractive (noncontact) force mode to image individual nanometer-size Au clusters preformed in the gas phase and deposited on a wide variety of atomically flat substrates. Using this noncontact technique, it is possible to reliably image preformed clusters in their as-deposited positions. This capability allows nanoindentation studies to measure the mechanical properties of individual nanometer-size Au clusters supported on atomically flat substrates and permits a measure of the deformation of a nanometer-size cluster as a function of the applied load. Applying a compression model to the deformed clusters, an elastic modulus roughly 2/3 that of bulk Au is obtained for annealed clusters with sizes between 3 and 18 nm. If the clusters are unannealed, a significantly smaller elastic modulus is observed (approximately 1/6 that of bulk Au). As the applied load increases beyond $\sim$ 20 nN, the data suggest that the yield point of an annealed Au cluster can be exceeded and the atomic force microscope tip can fracture the cluster.

I. INTRODUCTION

The general interest in the properties of supported, nanometer-size clusters has been motivated by a number of factors. Long-standing questions about the evolution of the atomic and electronic structure of nanometer-size objects as a function of size are starting to be addressed thanks to recent theoretical and experimental advances.[1,2] Experiments on the size-dependence of cluster melting have elucidated how classical thermodynamic concepts, applicable to the bulk, evolve as the system size decreases toward the atomic limit.[3,4] Similar information about the evolution of the electronic states of supported clusters has also been reported.[5–7] Interesting properties have been reported for bulk materials formed by consolidating nanoscale clusters.[8] In addition, while the properties of clusters and cluster-assembled materials are interesting in their own right, clusters also serve as potential building blocks for structures fabricated at the nanometer length scale. In essence, by studying the properties of supported clusters, we have a way to learn what unique properties nanoscale solid-state structures are likely to have.

A generic problem encountered in the study of supported clusters is the ability to probe the properties of individual clusters. Experiments that lack the spatial resolution to address the properties of a single cluster often yield confusing results because of the inherent convolution over cluster size and configuration. With the advent of the scanning probe microscopes, these concerns can, in principle, be addressed due to the high spatial resolution of the scanning probe technique. However, a problem encountered in many previous scanning probe studies of supported clusters is the difficulty in locating the clusters on atomically flat substrates. When clusters are deposited on rough substrates in an effort to reduce their mobility, the roughness restricts the ability to distinguish a supported cluster from the the rough substrate features.

The few successful studies of supported clusters reported have often focused on clusters formed by thermally evaporating metal atoms onto heated, atomically flat substrates. Diffusive motion of the deposited atoms produce raftlike structures often referred to as "clusters." An early example is a scanning tunneling microscope (STM) study of isolated atoms and rafts of Au, Ag, and Al in air on highly oriented pyrolytic graphite (HOPG).[9] Subsequent STM studies of these two-dimensional agglomerates have also been performed in ultrahigh vacuum (UHV) conditions, with atomic-scale features resolved on some of the raftlike structures.[10] Friction measurements and cluster geometry have also been determined using atomic force microscopy (AFM) studies of three-dimensional Pd clusters grown on mica.[11]

While such studies are useful for understanding the early stages of film formation on substrates, they provide little or no information on the unique properties of a cluster preformed in the gas phase and deposited on a substrate. A primary prerequisite for studying such a preformed, supported cluster on a substrate is a reliable method for producing large amounts of well characterized, nanometer-size clusters. In this regard, Andres and co-workers[12,13] have shown that using a multiple expansion gas aggregation source, clusters with a controlled mean-size and narrow-size distribution can be produced

and subsequently deposited onto a wide variety of substrates.

The first scanning probe study of these preformed nanometer-size clusters was reported by Baro *et al.* using STM and emphasized the importance of surface defects in trapping a small fraction of the deposited clusters.[14] Further studies have been reported for Au clusters supported on flat Au and Pt substrates.[4,15] An important result from this work was the discovery that step edges play an important role in trapping the individual clusters. A common problem encountered in these early studies was the difficulty in obtaining a scanning probe image of even a single preformed cluster, leading to the conclusion that preformed clusters have a high mobility on atomically flat substrates.

In a recent paper, this long-standing problem has been solved and a reliable way to image preformed nanometer-size metallic clusters on atomically-flat substrates using scanning probe techniques was reported.[16] Schaefer *et al.* have demonstrated that by using an AFM in the noncontact mode,[17,18] reliable images of deposited clusters on a wide variety of atomically-flat substrates can be achieved (see Fig. 1). This technique has the distinct advantage of revealing clusters in their as-deposited condition.

In what follows, we take advantage of this technique to locate clusters and then use the nanoindentation capabilities of the atomic force microscope to measure the deformation as a function of applied load for individual Au clusters supported on different atomically flat substrates. These studies allow a measure of the deformation of a nanometer-size cluster for applied forces as small as ~5 nN.

II. GROWTH AND CHARACTERIZATION OF GOLD CLUSTERS

A. Cluster source

A description of the multiple expansion cluster source (MECS) used in this study can be found in the literature.[12,13,4] It is a gas aggregation source, that is designed to run with 20 to 50 Torr of inert gas in the growth region. Both cluster growth via accretion of single atoms and via cluster-cluster aggregation can be promoted. In the present experiments, Au clusters with diameters as large as 20 nm were produced by aggregation of primary clusters with diameters in the 1 nm to 1.5 nm range. As in previous studies,[6,7,19–22] cluster samples were captured either on substrates for scanning probe analysis or on suitable amorphous carbon grids for further analysis by TEM. Previous TEM studies of clusters studied in this way have confirmed the ability of the MECS to produce metal clusters having a controlled mean-size and a narrow-size distribution.[12,13] For cluster samples with mean diameters less than 5 nm, the full width at half maximum is $\sim \pm 0.5$ nm, while for samples with larger mean diameter this width increases to $\sim \pm 1 - 2$ nm.

For the experiments on annealed clusters described below, the cluster aerosol was passed through a tubular annealing reactor consisting of a 2.54 cm diameter, 75 cm long, alumina tube passing through a Lindberg furnace. The mean residence time of a cluster in the tube is approximately one second and the pressure is 10 to 40 Torr. With this arrangement clusters passing from the growth

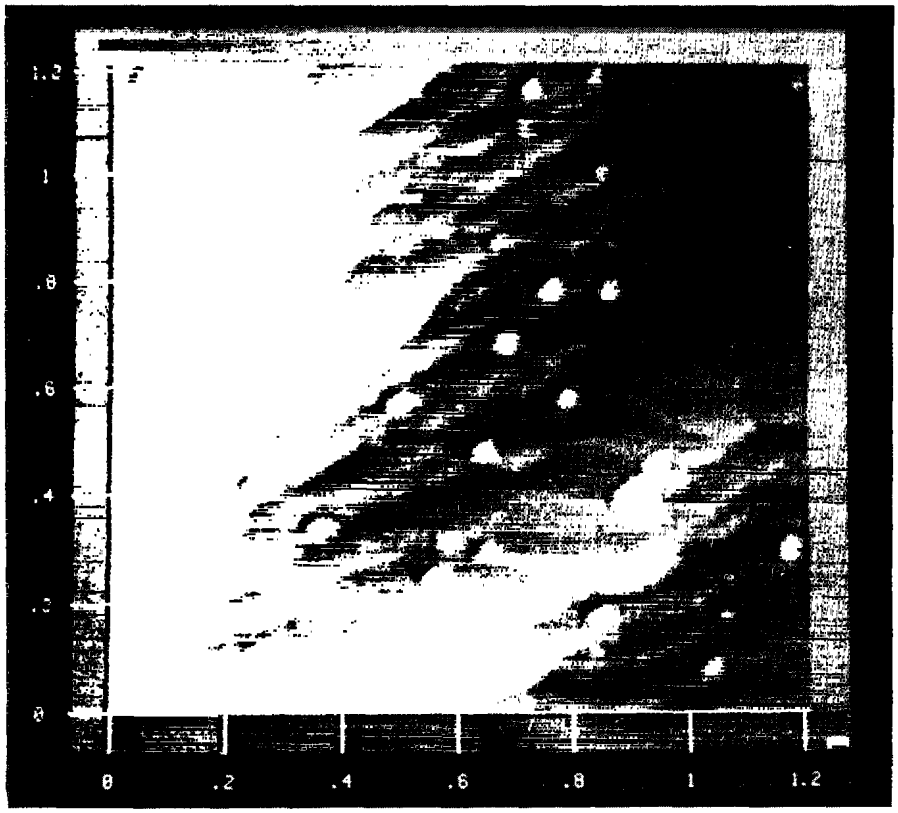

FIG. 1. Atomic force microscope image of gold clusters deposited onto an α-Al_2O_3 substrate. The image was taken using the noncontact imaging mode. Contact mode imaging proved to dislodge the clusters, producing images of only the bare substrate.

region of the MECS at 300 K could be heated to a predetermined temperature and then cooled again to 300 K. After annealing, the clusters pass into a vacuum chamber with a base pressure of 1×10^{-6} Torr and are deposited onto carbon coated TEM grids (carbon film thickness 5 nm) or a suitable substrate for future scanning probe studies.

B. Cluster structure and orientation

Previous high-resolution transmission electron microscopy (HRTEM) studies of the structure of annealed Au clusters have been reported as a function of the temperature of the annealing reactor.[23] The results of these experiments can be summarized as follows.

(1) Without annealing the MECS clusters are multiply twinned polycrystals with fcc domains between 1 and 2 nm in diameter.

(2) When the clusters are annealed at 1200 K (a temperature sufficient to melt Au clusters with diameters less than ~7.5 nm),[20] all clusters with diameters greater than ~ 8 nm were found to have a multiply twinned polycrystalline motif. Several symmetrical multiply twinned polycrystals (both icosahedra and decahedra) were observed. All clusters with diameters less than ~8 nm which were oriented in such a way as to show (111) lattice fringes were observed to be single fcc crystals.

(3) When the clusters are annealed at 1400 K (above the bulk melting temperature of Au), all clusters oriented in such a way as to show clear (111) lattice fringes could be unambiguously identified as single fcc crystals.

Figure 2 shows a representative TEM image of a typical annealed Au cluster sampled from the MECS cluster beam after passing through the annealing reactor held at 1400 K. The cluster is typical of the clusters used in the experiments reported below. The image clearly shows the lattice fringes associated with the Au atoms and indicates the clusters under study here are fcc crystals of polyhedron shape. The results of a systematic study of microdiffraction from thin films comprised of these individual clusters also show that a deposited cluster has a preferred orientation, with the [111] direction perpendicular to the substrate.

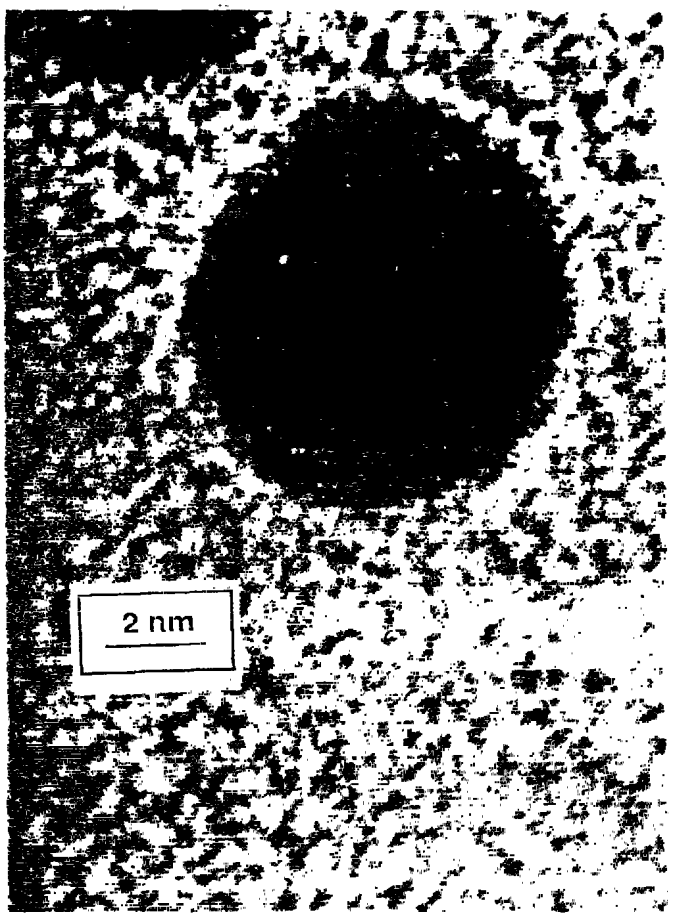

FIG. 2. High resolution TEM micrograph of a supported ~ 2 nm diameter Au cluster that was annealed in flight before deposition onto a thin carbon support grid. The lattice planes of the atoms comprising the cluster are clearly visible.

III. AFM CHARACTERISTICS

The AFM used was a custom-built instrument operating in either an ambient or vacuum environment and capable of scanning in either the contact or noncontact mode. Cluster-covered substrates are mounted onto a segmented, 1.27 cm long PZT-5A piezoelectric tube. A second piezoelectric tube is used to hold a commercially available AFM Si ultralever.[24] This second piezo tube allows for the oscillatory motion of the tip during noncontact operation and cantilever calibration. Detection of the cantilever displacement utilizes the laser deflection method[25,26] in which a focused laser beam is reflected off the back of the cantilever onto a split photodiode position sensing detector (PSD). The output of the PSD is read by a 68030 CPU based computer system. The computer handles all data acquisition and system control.

All noncontact mode scans were performed using an amplitude modulation technique. When the separation distance between the cantilever tip and substrate becomes $\leq$ 10 nm, attractive forces produce a shift in the cantilever resonant frequency, producing a change in the output of a lock-in amplifier. Digital feedback utilizing the lock-in output was used to keep the resonant frequency constant, corresponding to a constant separation between tip and substrate. When operating in the noncontact mode, the height resolution is ~ 0.2–0.5 nm, while the typical lateral resolution is estimated to be between 10 and 20 nm. The lateral resolution is, however, very dependent on the tip condition and can increase to over 100 nm after a tip crash.

One difficulty in using the AFM to do indentation experiments is the inherent hysteresis present in the piezo tubes. The nonlinear motion in the z direction distorts the slope of the indentation curves, leading to large errors and irreproducible results. It was determined that the nonlinearity becomes significant when tube displace-

ments exceed $\sim$ 10 nm. To overcome this problem, a correction system was installed which provided an independent measure of the sample displacement as a function of the z voltage applied to the piezo tube. This correction system consisted of a small mirror mounted onto the piezo tube near the sample mount. A laser photodiode was used to reflect a beam off the mirror, into a second PSD. The output was then used to linearize the sample motion through post-data acquisition analysis.

A second difficulty is a precise determination of the spring constant of each cantilever used in a nanoindentation experiment. Thickness variations have been reported[27] which cause an uncertainty in the spring constant from the manufacturer's specifications. To eliminate this problem, the vibrational spectrum of each cantilever was measured. From this spectrum, the resonance frequency ω_0 and a quality factor Q for each cantilever was determined. Using the measured value of ω_0, the spring constant of the lever was then calculated.[28] Typical values ranged from 2.2 N/m to 3.2 N/m.

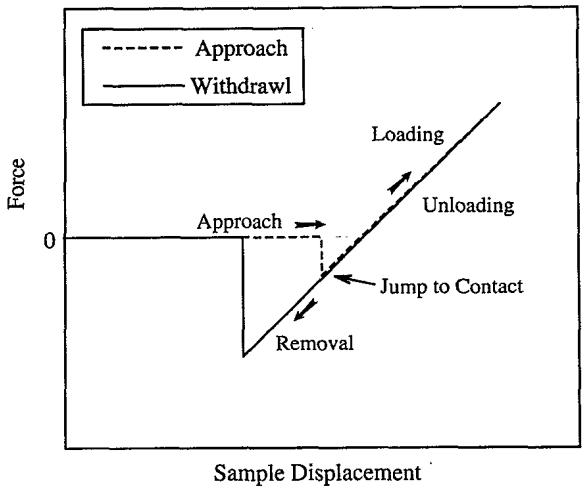

FIG. 4. A schematic contact mode force curve obtained during a nanoindentation experiment. The regions of interest are labeled in the figure.

IV. PROCEDURES

A. Calibration checks on bulk material

Before performing indentation experiments on individual clusters, considerable effort was made to check the overall reliability of the indentation capabilities of the scanning force instrument. Early studies were plagued by drift and hysteresis effects in the piezoelectric elements in the AFM. After correcting this problem by independently measuring the motion of both the sample and cantilever, reliable indentation studies on bulk materials became feasible.

The procedure for obtaining nanoindentation data is shown schematically in Figs. 3 and 4. After the sample was mounted in the AFM apparatus, the system is allowed to equilibrate for several hours. The sample is then brought to within $\sim$ 10 nm of the tip [see Fig. 3(a)]. At this point, the sample was moved forward in incremental steps toward the tip at a constant rate of $\sim$ 2 nm/s (see Fig. 3(b)). This constant rate was used for all

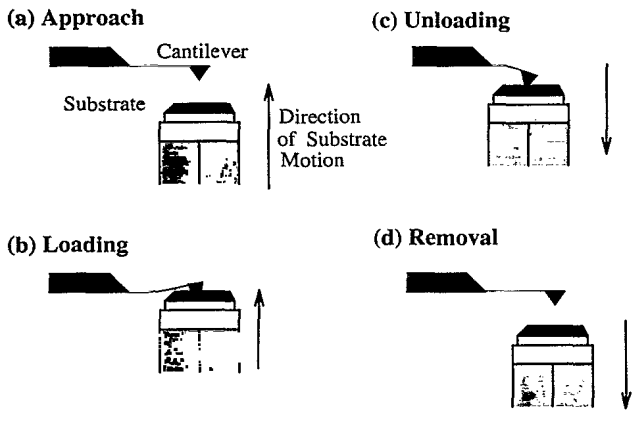

FIG. 3. Nanoindentation procedure followed to obtain contact mode force data.

experiments described and no experiments to determine a rate dependence were attempted. At each step, 25 data points were used to produce an average tip and sample position. The sample continued to move forward until a specified load was produced. The sample was then immediately withdrawn at the same rate as the approach, as depicted in Fig. 3(c). Loading values are determined by multiplying the displacement of the tip from its equilibrium position by the measured spring constant. The displacement of the tip must be determined very accurately, so a calibration is done before every experiment. The calibration is performed by using a sapphire disk to push on the cantilever. It is assumed that the tip and the sapphire disk move together with no deformation.

Figure 4 illustrates an ideal force curve produced using this technique. The curve can be described in terms of three distinct regions; a jump to contact region, a loading-unloading region, and a removal region. The jump to contact region provides information about the long range attractive forces between the AFM tip and the surface. The elastic properties of the material can be determined from the loading-unloading region, which contains information about the deformation of the object under study.[29,30] The removal region provides information about the adhesion between the AFM tip and the surface.

The instrument and calibration procedures were checked by studying the mechanical properties of an elastomer and bulk Au for large ($\sim$ 200 nN) and small ($\leq$ 100 nN) loads in air and vacuum. These two materials were chosen because they span the range of elastic properties of interest in this study. Also, previous studies of these materials have been reported in the literature,[29] thereby allowing a cross check on the procedures employed here.

An analysis of the force data requires a knowledge of the penetration distance of the tip into the substrate. The penetration depth, h, was determined by

$$h = z_{\text{sample}} - z_{\text{tip}}, \tag{1}$$

where z_{sample} and z_{tip} are the measured positions of the sample and tip in the region of positive applied load. The elastic modulus of the substrate can be calculated from the slope, S, of the unloading curve plotted as a function of penetration depth. The standard equation for an axisymmetric indenter,[30]

$$S = \frac{dP}{dh} = \beta E^*_{sub}\sqrt{A}, \tag{2}$$

was used, where β is a constant which depends on the geometry of the tip, A is the projected contact area of the indenter, and E^*_{sub} is the reduced elastic modulus of the tip substrate given by

$$\frac{1}{E^*_{sub}} = \frac{(1-\nu^2_{substrate})}{E_{substrate}} + \frac{(1-\nu^2_{tip})}{E_{tip}}. \tag{3}$$

The hardness, H, was determined according to the standard definition,[30]

$$H = \frac{F_{max}}{A}. \tag{4}$$

The relevant contact area for each tip was estimated in two separate ways. The first method relied on indentation data obtained from HOPG, which in this case was treated as a substrate with known elastic properties. From Eq. (2), a constant slope S implies a constant contact area. This behavior was observed in our experiments.[31] We, therefore, modeled the tip as an axisymmetric indenter with cylindrical symmetry. Using Eq. (2) and β=1.129 (circular contact area),[32] $E_{HOPG} = 17$ GPa,[33] $E_{tip} = 60$ GPa (SiO_2),[34] and $\nu_{HOPG} = \nu_{tip} = 0.3$, the contact area for each tip could be inferred.

As a check on this procedure, TEM was used to determine the tip profile. Using a Hertzian model, a spherical tip of radius R_{tip} elastically contacting a flat surface under an applied force F has a contact area given by

$$A_{con} = \pi\left(\frac{3FR_{tip}}{4E^*_{sub}}\right)^{\frac{2}{3}}. \tag{5}$$

Contact areas determined in this way were compared to those determined from indentation on HOPG. By combining these two techniques, a reliable estimate for the contact area was found in each case.

The results of the bulk measurements have been reported in the literature,[35] and are summarized in Table I. From these checks on bulk materials, it was concluded that the AFM was stable and reliable enough to be used in cluster nanoindentation studies.

TABLE I. Comparison of measured elastic properties of an elastomer and bulk gold with literature values.

Source	Material	Elastic modulus	Hardness
Measured	elastomer	8.2 GPa	
Literature[29]	elastomer	10 GPa	
Measured	bulk gold	79 GPa	0.69 N/m^2
Literature[29]	bulk gold	80 GPa	0.65 N/m^2

B. Substrates

A variety of substrates were considered for use in this study. Initially, the binding of the gold clusters to HOPG substrates was found to be weak,[31] requiring light loading forces ($\leq$ 10 nN) to perform a successful indentation test. Larger loading forces tended to dislodge the cluster, with the result that the cluster was moved out from under the tip during the indentation measurement. Therefore, other substrates which bind Au clusters more strongly were considered.[36] It was for this reason that substrates like α-Al_2O_3 and mica were selected. A second concern was the effects of contamination when performing these tests in ambient conditions. Contamination effects have been observed to greatly effect the adhesion and initial contact regions of AFM force data, although the loading and unloading regions are not believed to be greatly influenced. To address the contamination issue, force measurements were performed under moderate vacuum conditions ($\sim$ 0.6 Torr). At these pressures, surface effects due to volatile adsorbates are minimized.

The properties of α-Al_2O_3 make it an ideal substrate for performing force measurements on clusters. The surface has many atomically flat areas which allow clusters to be imaged. Large surface forces due to the high surface energy of α-Al_2O_3 (0.85 J/m^2) also tend to bind the clusters strongly to the substrate. This facilitates the use of larger loading forces during indentation. Also, since the elastic modulus of α-Al_2O_3 is 400 GPa,[30] substrate deformation is minimized when performing nanoindentation measurements on supported clusters. The ability to prepare atomically flat substrates of α-Al_2O_3 is also an important consideration for this study.[37,36] It is easy to prepare atomically flat mica surfaces by cleaving. Mica also binds Au clusters well and has a high elastic modulus (179 GPa).

C. Cluster indentation analysis

The procedure followed when performing force measurements on clusters was similar to that described elsewhere.[31] The elastic properties of a supported cluster were measured by (i) locating a cluster using the noncontact mode of operation, (ii) removing the oscillatory motion of the cantilever, (iii) positioning the tip over the cluster, (iv) moving the sample toward the Si tip on the cantilever until a specified indentation force was reached, and (v) withdrawing the sample from the cantilever.

Immediately after measuring the deformation of the cluster under loading, a calibration curve was obtained by performing a nanoindentation on the substrate close to the cluster. This served several purposes. First, it was used to distinguish between a successful and unsuccessful indentation on a cluster. If the tip misses the cluster, the resulting nanoindentation data are characteristic of the substrate. If the tip successfully comes down on the cluster, the nanoindentation data will possess characteristics unique to a gold cluster. Second, the substrate acts as a calibration of the tip contact area if properties of the substrate are known.

A quantitative analysis of the data depends on whether the contact area of the tip is larger or smaller than the top facet of the cluster. If the contact area of the tip is much smaller than the cluster face, Eq. (2) can be used with the contact area being determined by the tip. If the contact area of the tip is larger than the cluster face, the tip can be approximated as a flat plate and the contact area will be that of the cluster face. In any case, an accurate estimation of the contact area is of considerable interest.

It follows that a judgement must be made about the size of the tip relative to the cluster under study. This requires information about cluster shape. As discussed in Sec. IIB above, microdiffraction TEM studies have shown that annealed Au clusters have a strong tendency to orient on a substrate with the [111] direction normal to the surface of the substrate. Thus, to quantitatively analyze the nanoindentation data from a single cluster, it becomes necessary to estimate the area of the (111) facet of the cluster. To do this, the area of the (111) face of a perfect closed shell cluster as a function of cluster height h_{cl} was calculated. As an example, a gold cluster containing 1289 atoms has a height of 2.8 nm and a face area of 4.40 nm^2. Likewise, an Au cluster with 2406 atoms has a height of 3.5 nm and a face area of 6.55 nm^2. Thus, for a cluster with a height of say 3.1 nm, it is reasonable to assume that $4.4\ nm^2 \leq A_{cl} \leq 6.55\ nm^2$.

For the cluster indentation experiments reported below, the contact area of each tip, determined by measuring R_{tip} from TEM micrographs and using this value in Eq. (5) to analyze indentation data from the appropriate substrate, was greater than the area of the cluster face as calculated from the measured height of the cluster following the procedure described above. Based on this result, the analysis of the cluster nanoindentation data can best be described using a compression model in which the relevant contact area is determined by A_{cl}, the area of the top face of the cluster.

The measured deformation of the cluster is assumed to consist of three contributions: (i) the deformation of the cluster-tip interface, (ii) the compression of the cluster itself along its [111] direction, and (iii) deformation of the cluster-substrate interface. The compression of the cluster is modeled by the expression

$$\frac{F}{A_{cl}} \equiv E_{cl}\frac{\Delta h_{cl}}{h_{cl}}, \tag{6}$$

where E_{cl} is the elastic modulus of the cluster, Δh_{cl} is the deformation of a cluster with a height h_{cl}. Δh_{cl} can be related to the measured deformation Δh_m using

$$\Delta h_{cl} = \Delta h_m - \Delta l_{substrate} - \Delta l_{tip}, \tag{7}$$

where $\Delta l_{substrate}$ and Δl_{tip} are the deformations of the substrate and tip interfaces, respectively. Combining Eqs. (6) and (7) and using Eq. (2) (appropriately modified) to estimate $\Delta l_{substrate}$ and Δl_{tip}, we find that the elastic modulus of the cluster is given by

$$E_{cl} = \frac{\frac{h_{cl}}{A_{cl}} + \frac{2(1-\nu_{cl}^2)}{\beta\sqrt{A_{cl}}}}{\frac{1}{S} - \frac{1}{E^*_{sub}\beta\sqrt{A_{cl}}}}, \tag{8}$$

where $S = F/\Delta h_m$ is measured from the force vs deformation data.

V. RESULTS

A. Jump-to-contact and lift-off behavior

Force curves obtained from a single gold cluster and from the substrate are qualitatively and quantitatively different, allowing an easy determination of whether any given indentation is actually performed on a selected cluster. To illustrate this point, representative force curves on an α-Al_2O_3 substrate and on a gold cluster on α-Al_2O_3 are shown in Fig. 5. Each curve appears qualitatively different in the jump to contact and removal regions.

For the α-Al_2O_3 substrate, the tip jumps to contact and immediately retreats backward to the position be-

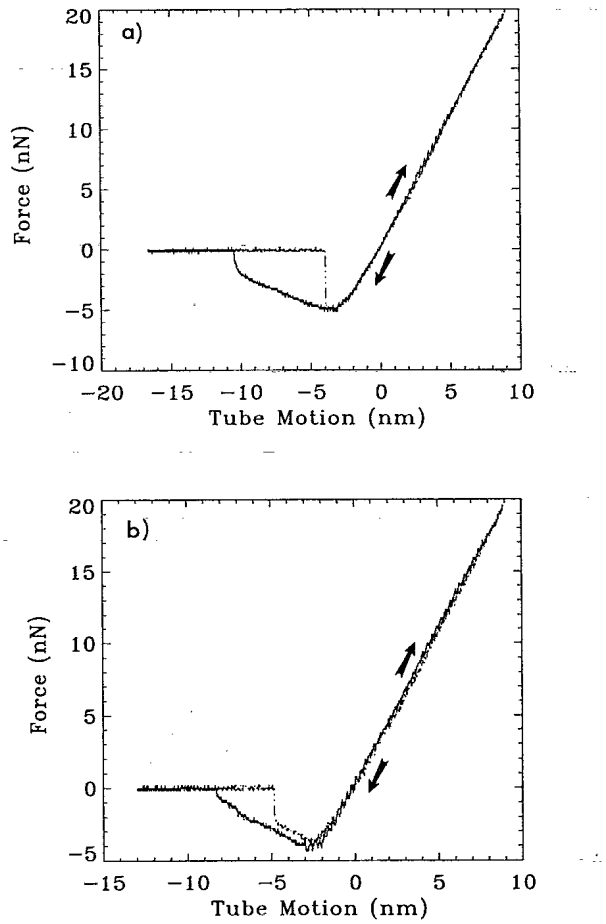

FIG. 5. Representative force curves on (a) α-Al_2O_3 and (b) a 4.5 nm high Au cluster on an α-Al_2O_3 substrate. Both curves are taken in moderate (0.6 Torr) vacuum conditions. The spring constant of the cantilever is k= 3.24 N/m; the tip radius is $R_{tip} \simeq 20$ nm.

fore the jump to contact occurred, indicating that no contamination is present on the surface. For the gold cluster, however, the tip jumps to contact and continues to move forward in a manner similar to that seen in force measurements on bulk gold under vacuum conditions[38] (see Fig. 6). After initially contacting the surface of the cluster, the tip continues to move forward for ~ 0.3 nm before reversing its motion.[39] As with bulk gold, this behavior is attributed to a bridge between the tip and cluster formed by mobile gold surface atoms.[40] The removal curves are also qualitatively different. The α-Al_2O_3 data show more curvature during release, while the data from an Au cluster appears linear. The cluster pull-off curve is also observed to initially parallel the contact data (they overlap in many data runs), a behavior often observed in bulk gold studies.

A substantial contamination layer is not expected to be present on Au clusters on α-Al_2O_3 and mica in vacuum. Thus, quantitative comparisons can be made between the jump to contact on the cluster and on the α-Al_2O_3 and mica substrates. The data for annealed Au clusters are summarized in Tables II and III. In these tables, the jump to contact distance z_{jtc} is determined by dividing the measured abrupt change in force when the cantilever jumps by the known spring constant of the cantilever. From this data, we find that the tip systematically jumps to contact at a distance closer to the surface of the cluster than it does for the bare substrate.

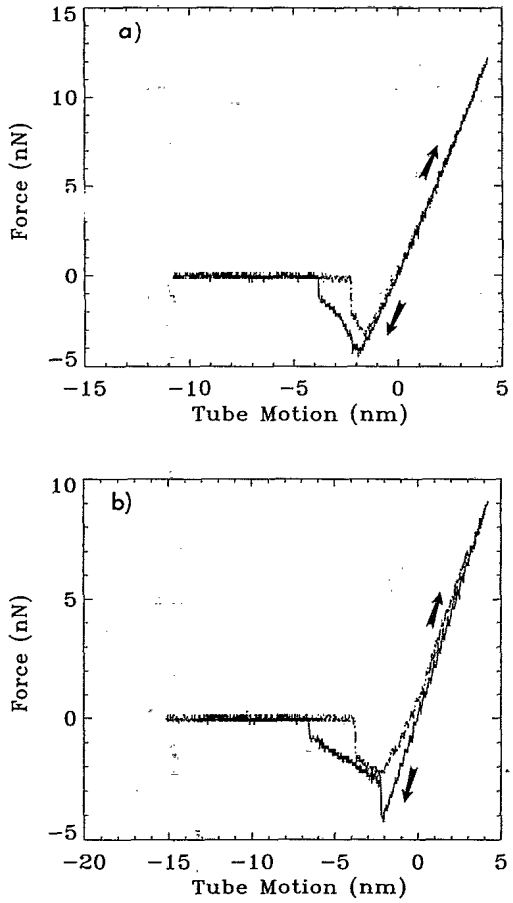

FIG. 6. A comparison of (a) a force curve taken on bulk gold using a cantilever with a spring constant k=3.3 N/m having a tip radius $R_{tip} \simeq 40$ nm and (b) a force curve obtained on a 7.2 nm high gold cluster on an α-Al_2O_3 substrate using a cantilever with a spring constant k=3.20 N/m having a tip radius $R_{tip} \simeq 10$ nm. Both curves are taken in moderate (0.6 Torr) vacuum conditions.

TABLE II. Jump to contact distances (z_{jtc}) and removal force from nanoindentation data on annealed Au clusters supported on α-Al_2O_3. For purposes of comparison, similar data from bare α-Al_2O_3 substrate are also included.

Material	Size (nm)	z_{jtc} (nm)	Removal force (nN)	Max. loading force (nN)
Au cluster	4.5	1.1 ± 0.2	6.9 ± 0.7	$20 - 39$
Al_2O_3		2.0 ± 0.2	7.6 ± 0.3	$20 - 39$
Au cluster	4.9	1.4 ± 0.1	5.7 ± 0.3	21.7 ± 0.3
Al_2O_3		2.4 ± 0.1	8.0 ± 0.4	21.6 ± 0.2
Au cluster	5.0	1.1 ± 0.2	6.9 ± 0.5	21.1 ± 0.2
Al_2O_3		2.0 ± 0.1	7.1 ± 0.1	21.3 ± 0.3
Au cluster	5.2	1.3 ± 0.1	6.8 ± 0.5	21.0 ± 0.2
Al_2O_3		1.6 ± 0.2	6.5 ± 0.2	21.2 ± 0.1
Au cluster	10.9	1.1 ± 0.1	4.7 ± 0.1	21.8 ± 0.2
Al_2O_3		2.3 ± 0.1	8.0 ± 0.3	21.9 ± 0.3
Au cluster	11.1	0.9 ± 0.1	6.1 ± 0.2	21.4 ± 0.2
Al_2O_3		2.4 ± 0.2	8.0 ± 0.5	21.2 ± 0.3
Au cluster	11.7	1.1 ± 0.1	5.2 ± 0.5	$20 - 47$
Al_2O_3		2.5 ± 0.1	8.6 ± 0.2	$20 - 47$
Au cluster	17.2	0.8 ± 0.1	4.7 ± 0.3	$20 - 30$
Al_2O_3		2.1 ± 0.1	7.8 ± 0.6	$20 - 30$

This systematic trend can be understood by realizing that jump to contact will occur when the surface interaction force gradient exceeds the spring constant of the lever. Assuming a van der Waals interaction, the jump to contact distance, z_{jtc}, is given by

$$z_{jtc} = \left(\frac{HR}{6k}\right)^{\frac{1}{3}} \tag{9}$$

where H is the Hamaker constant, k is the spring constant, and R is the effective radius of the system given by

$$R = \frac{R_{tip} R_{sample}}{R_{tip} + R_{sample}}. \tag{10}$$

TABLE III. Jump to contact distances (z_{jtc}) and removal force from nanoindentation data on annealed Au clusters supported on mica. For purposes of comparison, similar data from bare mica substrate are also included.

Material	Size (nm)	z_{jtc} (nm)	Removal force (nN)	Loading force (nN)
Au cluster	13.5	0.5 ± 0.1	3.2 ± 0.5	$19 - 30$
Mica		1.2 ± 0.2	5.6 ± 0.6	$19 - 30$
Au cluster	18.1	2.2 ± 0.2	9.0 ± 0.2	12.2 ± 0.1
Mica		1.9 ± 0.1	8.5 ± 0.5	12.4 ± 0.1

In Eq. (10), R_{sample} refers to the cluster or the substrate, depending upon the placement of the tip. From this analysis, the jump to contact distance is expected to scale roughly as $R^{\frac{1}{3}}$.

When the tip is positioned over an atomically flat substrate, $R_{\text{sample}} = \infty$ and $R = R_{\text{tip}}$. When the tip is over a cluster, the small radius of curvature of the cluster yields $R < R_{\text{tip}}$. Therefore, the jump to contact distance when a tip is over the cluster should generally be smaller than when the tip is approaching a flat substrate, assuming the Hamaker constant is comparable in both cases. This is indeed observed. Equation (9) also predicts a cluster size dependence in the jump to contact distance which is not observed, possibly due to uncertainties in the measurements.

The data also indicate that the removal force is systematically lower on the cluster than on the substrate. According to Johnson, Kendall, and Roberts (JKR) theory,[41] the removal force is given by

$$F_{\text{rem}} = 3\pi R\sqrt{\gamma_{\text{tip}}\gamma_{\text{sample}}}. \quad (11)$$

Since $\gamma_{\text{gold}} = 1.4$ J/m^2, $\gamma_{Al_2O_3} = 0.85$ J/m^2, and $\gamma_{\text{mica}} = 0.3$ J/m^2, a conclusion might be made that the removal force from an Au cluster should be larger than from the substrate. However, as previously mentioned, the effective radius R is smaller when the tip is over a cluster. The average removal force for the silicon tip from a gold cluster was ~ 5.9 nN. For tip removal from the Al_2O_3 substrate, an average force of ~ 7.7 nN was required. Although, the observed trend agrees qualitatively with JKR theory, the removal forces are about an order of magnitude lower than predicted by JKR theory for both cluster and substrate. Such discrepancies have been observed in previous adhesion experiments with the AFM[42] and are believed to be due to uncertainties in the contact area and contamination effects.

B. Elastic modulus—annealed clusters

The slopes of the loading-unloading regions of the nanoindentation data obtained from different annealed Au clusters were analyzed and Eq. (8) was used to determine the elastic modulus of several nanometer-size clusters. Figure 7 shows a plot of the cluster modulus obtained in this way as a function of cluster size. Representative error bars reflect the uncertainty in determining the contact area. The measured values of the elastic modulus for Au clusters on HOPG, α-Al_2O_3, and mica are consistent, leading to the conclusion that possible surface contamination effects are minimal. While there is a general tendency for the measured modulus to increase with size, the uncertainties in the measurements prevents an unequivocal determination of whether a size dependence indeed exists. It is interesting to note that the modulus of the annealed clusters is about 2/3 that expected for bulk Au(111).

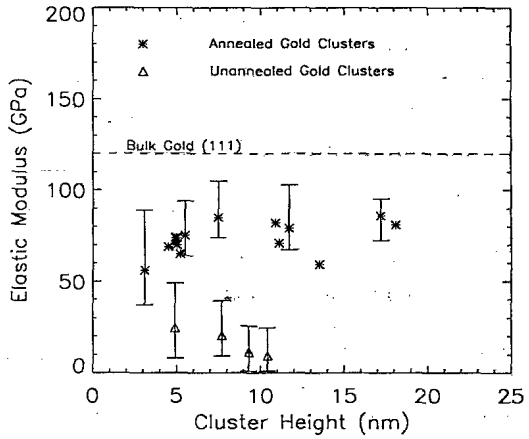

FIG. 7. Plot comparing the measured elastic modulus of unannealed gold clusters with the measured values on annealed gold clusters. For comparison, the bulk elastic modulus of Au(111) is also indicated.

C. Elastic modulus—unannealed clusters

Following the same procedure discussed above, unannealed Au clusters on an HOPG substrate were studied. As with the force curves on annealed clusters, the determination of a successful indentation was determined by comparing the results on the cluster with that from the substrate. Again, the jump to the contact distance and the removal force are observed to be lower for the cluster than the substrate. These results are summarized in Table IV.

Applying the same model as in previous sections, the elastic moduli for several unannealed clusters were determined and are plotted in Fig. 7. The elastic moduli of the unannealed clusters are found to be significantly lower than those measured for the annealed clusters. Unannealed clusters are known to be polycrystalline containing twin boundaries.[23] Therefore, we conclude that the existence of these defects in the clusters act to lower the elastic modulus significantly. This is in agreement with the observed plastic deformation of unannealed gold clusters deposited on flat gold substrates.[15]

TABLE IV. Jump to contact distances (z_{jtc}) and removal force from nanoindentation data on unannealed Au clusters supported on HOPG. For purposes of comparison, similar data from the bare HOPG substrate are also included.

Material	Size (nm)	z_{jtc} (nm)	Removal force (nN)	Max. loading force (nN)
Au cluster	4.9	0.7 ± 0.2	4.3 ± 0.7	7.1 ± 0.2
HOPG		2.3 ± 0.1	8.6 ± 0.6	7.1 ± 0.2
Au cluster	7.7	0.6 ± 0.1	5.0 ± 0.1	7.0 ± 0.1
HOPG		2.3 ± 0.1	8.8 ± 1.3	7.1 ± 0.1
Au cluster	9.3	0.7 ± 0.1	3.7 ± 0.2	7.1 ± 0.1
HOPG		2.2 ± 0.1	7.9 ± 0.7	7.1 ± 0.1
Au cluster	10.4	0.4 ± 0.1	3.6 ± 0.2	7.1 ± 0.1
HOPG		2.2 ± 0.1	8.5 ± 0.6	7.1 ± 0.2

A major difference in the force data between annealed and unannealed clusters was the evidence for plastic deformation of the unannealed clusters. Figure 8 shows representative force data from a 7.7 nm high unannealed gold cluster. Note the characteristic jump to the contact region of the force curve which corresponds to that seen with other gold clusters. A significant hysteresis is observed in the loading and unloading curves, however, signifying the presence of inelastic processes. Force data on the HOPG substrate showed no inelastic effects, indicating that the tip was not inelastically deforming. This hysteresis is observed in about 75% (18 of 24) of the force curves taken on unannealed clusters, while less than 12% (23 of 198) of the force curves on annealed clusters show this effect. Similar features have been observed in molecular dynamics calculations for a diamond tip indenting a Cu (111) surface.[43]

It is also apparent from Fig. 8 that there are a number of sudden decreases in the applied force during the loading portion of the curve, indicating a yielding of the surface due to inelastic processes. The two large jumps evident in Fig. 8 correspond to tip displacements of ~ 0.65 nm, corresponding to about twice the distance between (111) planes in Au.[44] These jumps have been predicted from molecular dynamics simulations for a diamond tip indenting a Cu(111) surface and correspond to atoms "popping" out from under the tip onto the metal surface.[43]

Two different behaviors are typically observed in the removal data for the unannealed clusters. As observed in Fig. 8, in some cases the tip reaches a minimum force and slowly releases from the cluster. During this release, several jumps in the data indicate the release of individual atoms or groups of atoms between the tip and cluster. The release continues until the tip totally separates from the cluster and returns to its equilibrium position. A different effect is shown in Fig. 9. In the unloading region, the load is observed to initially decrease linearly as the sample is withdrawn. At some point, however, the tip experiences an upward deflection, indicating that positive loads are being applied by the tip. This effect was

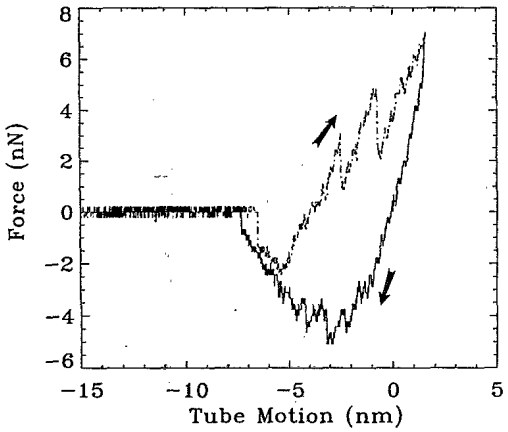

FIG. 8. Force curve taken on an unannealed cluster with a height of 7.7 nm on an HOPG substrate. The abrupt cantilever displacements are attributed to plastic deformation. The spring constant of the cantilever is $k = 3.17$ N/m; the tip radius is $R_{\text{tip}} \simeq 10$ nm.

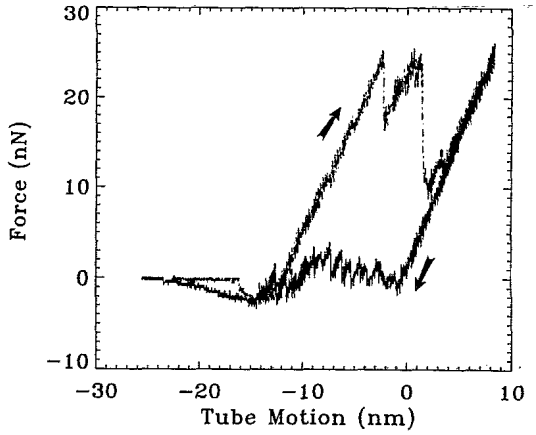

FIG. 9. Force curve taken on an annealed cluster with a height of 13.5 nm on a mica substrate. The data provide evidence for plastic deformation. The spring constant of the cantilever is $k = 3.22$ N/m; the tip radius is $R_{\text{tip}} \simeq 10$ nm.

also observed in molecular dynamics simulations,[43] and is attributed to a reconstruction of the surface atoms, returning the surface into more intimate contact with the tip. The contact between the surface and tip produces the positive loads observed in Fig. 9.

Images of the cluster were obtained both before and after these force curves were taken. Interestingly, no permanent cluster deformation was observed. One possible explanation for this is that the resolution of the AFM in noncontact mode is not high enough to resolve the deformation. Another explanation could be that any tip-induced deformations are quickly annealed out due to the high surface forces present in the nanoscale clusters.[40]

D. Deformation of an annealed cluster at high loads

The majority of the force curves on annealed gold clusters were found to exhibit purely elastic behavior. Occasionally, the pressure exerted by the tip exceeded the yield stress of the cluster, and plastic effects were subsequently observed. Figure 10 shows an example of a possible "fracturing" of a cluster with the AFM tip. Figure 10(a) shows an AFM noncontact scan of a 5.7 nm high gold cluster on HOPG. Immediately after the scan, the oscillatory motion of the tip was stopped, the tip was placed over the cluster, and an indentation test was performed. The resulting force data is shown in Fig. 10(b). The sudden drop in the loading data at an applied load of 30 nN was initially attributed to the cluster becoming dislodged and moving out from under the tip. However, the succeeding scan of the cluster [see Fig. 10(c)] showed a permanent deformation of the cluster. A scan of a neighboring cluster was then performed in order to check for the formation of a double tip. No double tip effects were seen, leading to the conclusion that the cluster had been deformed and not the tip. If the 30 nN force is applied uniformly across the face of the cluster, a lower limit for the applied stress of ~ 2 GPa is obtained. Another possible explanation for this result is that the cluster first scanned was really two closely spaced clusters that could not be reolved using the noncontact AFM. Under this cir-

cumstance, the AFM tip would have separated the two clusters, rather than causing the fracture of an individual cluster. The data would then provide information about the force needed to separate two clusters in close contact.

VI. CONCLUSIONS

It has been demonstrated that using an atomic force microscope in the noncontact mode, preformed nanometer-size Au clusters deposited onto atomically flat substrates can be reliably imaged in their as-deposited condition. Cluster sizes and coverages inferred from such studies are roughly comparable to those observed on simultaneously exposed TEM grids. Using the AFM as a nano-indentation device, the mechanical properties of individual nanometer-size clusters were investigated.

Both annealed and unannealed Au clusters were studied on atomically flat HOPG, mica, and α-Al_2O_3 substrates. For applied loads less than $\sim$ 20 nN, an elastic modulus roughly 2/3 of bulk Au was obtained for annealed Au clusters ranging in size from 3 to 18 nm

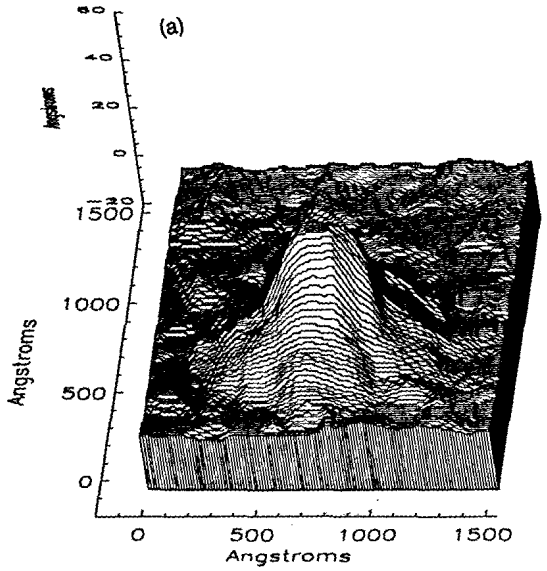

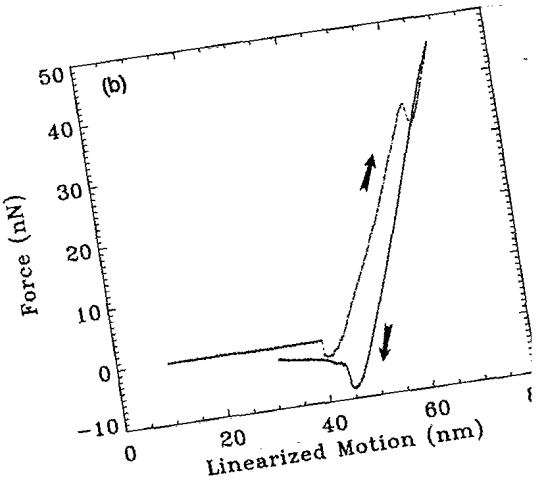

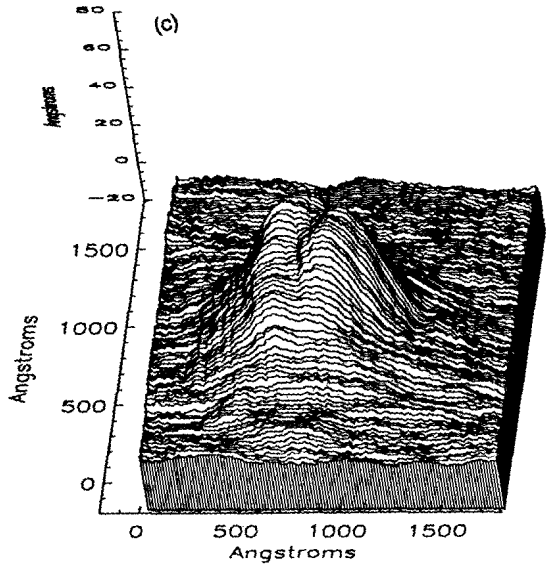

FIG. 10. (a) Initial noncontact AFM image of a annealed gold cluster (5.7 nm high) on HOPG b
we on the cluster showing a sudden decrease in the force applied by the tip.
dius is $R_{tip} \simeq 30$ nm. (c) A noncontact AFM image of th
ation of the cluster.

For unannealed Au clusters, a modulus roughly 1/6 of bulk Au was found. As the applied load increases above $\sim$ 20 nN, evidence was found that the yield point of an annealed Au cluster can be exceeded, resulting in a fracture of the cluster by the AFM tip.

Utilizing the noncontact imaging mode, further studies on individual nanometer-size clusters are now possible. Using the AFM to measure lateral forces provides the ability to measure the binding force between an individual cluster and a substrate. As a consequence of the high lateral resolution of the AFM, it also becomes feasible to quantitatively measure the binding force of individual preformed clusters to different substrates and defect sites.

ACKNOWLEDGMENTS

This work was partially funded by the National Science Foundation under Contract No. ECS-9117691.

[1] *Physics and Chemistry of Finite Systems: From Clusters to Crystals*, edited by P. Jena, S.N. Khanna, and B.K. Rao, (Kluwer Academic, Boston, 1992), Vols. I and II.
[2] *Small Particles and Inorganic Clusters*, edited by R.S. Berry, J. Burdett, and A.W. Castleman [Z. Phys. D **26** (1993)].
[3] Ph. Buffat and J.P. Borel, Phys. Rev. A **13**, 2287 (1976).
[4] T. Castro, Y.Z. Li, R. Reifenberger, E. Choi, S.B. Park, and R.P. Andres, J. Vac. Sci. Technol. A **7**, 2845 (1989).
[5] M.E. Lin, R.P. Andres, and R. Reifenberger, Phys. Rev. Lett. **67**, 477 (1991).
[6] M.E. Lin, R. Reifenberger, and R.P. Andres, Phys. Rev. B **46**, 15 490 (1992).
[7] M.E. Lin, R. Reifenberger, A. Ramachandra, and R.P. Andres, Phys. Rev. B **46**, 15 498 (1992).
[8] R.W. Siegel, Mater. Sci. Eng. B **19**, 37 (1993).
[9] D.W. Abraham, K. Sattler, E. Ganz, H.J. Mamin, R.E. Thomson, and J. Clark, Appl. Phys. Lett. **49**, 853 (1986).
[10] A. Humbert, M. Dayez, S. Granjeaud, P. Ricci, C. Chapon, and C.R. Henry, J. Vac. Sci. Technol. B **9**, 804 (1991).
[11] J. Colchero, O. Marti, J. Mlynek, A. Humbert, C.R. Henry, and C. Chapon, J. Vac. Sci. Technol. B **9**, 794 (1991).
[12] Seung Bin Park, Ph.D. thesis, Purdue University, 1988.
[13] E. Choi and R.P Andres, in *Physics and Chemistry of Small Clusters*, edited by P. Jena, B.K. Rao, and S.N. Khanna (Plenum Press, New York, 1987), p. 61.
[14] A.M. Baro, A. Bartolome, L. Vazquez, N. Garcia, R. Reifenberger, E. Choi, and R.P. Andres, Appl. Phys. Lett. **51**, 1594 (1987).
[15] Y.Z. Li, R. Reifenberger, E. Choi, and R.P. Andres, Surf. Sci. **250**, 1 (1991).
[16] D.M. Schaefer, A. Ramachandra, R.P. Andres, and R. Reifenberger, Z. Phys. D **26**, S249 (1993).
[17] Y. Martin, C.C. Williams, and H.K. Wickramasighe, J. Appl. Phys. **61**, 4723 (1987).
[18] G.M. McClelland, R. Erlandsson, and S. Chiang, Rev. Prog. Quant. Nondestruct. Eval. **6**, 1307 (1987).
[19] T. Castro, R. Reifenberger, E. Choi, and R.P. Andres, Surf. Sci. **234**, 43 (1990).
[20] T. Castro, R. Reifenberger, E. Choi, and R.P. Andres, Phys. Rev. B **42**, 8548 (1990).
[21] T. Castro, E. Choi, Y.Z. Li, R.P. Andres, and R. Reifenberger, in *Clusters and Cluster-Assembled Materials*, edited by R.S. Auerback, J. Bernholc, and D.L. Nelson, MRS Symposia Proceedings No. 206 (Materials Research Society, Pittsburgh, 1991), pp. 159–168.
[22] M.E. Lin, A. Ramachandra, R.P. Andres, and R. Reifenberger, in *Nanosources and Manipulation of Atoms under High Fields and Temperatures: Applications*, edited by B. Vu Thein, N. Garcia, and K. Dransfeld (Kluwer Academic Publishers, Boston, 1993), pp. 77–88.
[23] A.N. Patil, D.Y. Paithankar, N. Otsuka, and R.P. Andres, Z. Phys. D **26**, 135 (1993).
[24] Available from Park Scientific Instruments, Sunnyvale, CA 94089.
[25] G. Meyer and N.M. Amer, Appl. Phys. Lett. **53**, 1045 (1988).
[26] G. Meyer and N.M. Amer, Appl. Phys. Lett. **53**, 2400 (1988).
[27] H.J. Butt, P. Siedle, K. Seifert, K. Fendler, T. Seeger, E. Bamberg, A.L. Weisenhorn, K. Goldie, and A. Engel (unpublished).
[28] J.P. Cleveland, S. Manne, D. Bocek, and P.K. Hansma, Rev. Sci. Instrum. **64**, 403 (1993).
[29] N.A. Burnham and R.J. Colton, J. Vac. Sci. Technol. A **7**, 2906 (1989).
[30] W.C. Oliver and G.M. Pharr, J. Mater. Res. **7**, 1564 (1992).
[31] D.M. Schaefer, A. Patil, R.P. Andres, and R. Reifenberger, Appl. Phys. Lett. **63**, 1492 (1993).
[32] R.B. King, Int. J. Solids Struct. **23**, 1657 (1987).
[33] M.N. Gardos, *Mechanics of Coatings Tribology Series 17* (Elsevier, Amsterdam, 1989).
[34] Dror Sarid, *Scanning Force Microscopy* (Oxford University Press, New York, 1991).
[35] D.M. Schaefer, A. Patil, R.P. Andres, and R.R. Reifenberger, in *Proceedings of the 1993 AFM/STM Symposium at the U.S. Army Natick Laboratory*, edited by S.H. Cohen, M. Bray, and M. Lightbody (Plenum, New York, 1995), pp. 411–421.
[36] W. Mahoney, D.M. Schaefer, A. Patil, R.P. Andres, and R. Reifenberger, Surf. Sci. **316**, 383 (1994).
[37] M.G. Norton, S.R. Summerfelt, and C.B. Carter, Appl. Phys. Lett. **56**, 2246 (1990).
[38] D.M. Schaefer and R. Reifenberger, in *Determining Nanoscale Physical Properties of Materials by Microscopy and Spectroscopy*, edited by M. Sarikaya, M. Isaacson, and H.K. Wickramasighe, MRS Symposia Proceedngs No. 332 (Materials Research Society, Pittsburgh, 1993), pp. 225–230.
[39] The tip motion is calculated from the change in force divided by the known spring constant of the cantilever.
[40] J.I. Pascual, J. Mendez, J. Gomez-Herrero, A.M. Baro, N. Garcia, and Vu Thien Binh, Phys. Rev. Lett. **71**, 1852 (1993).
[41] K.L. Johnson, K. Kendall, and A.D. Roberts, Proc. R. Soc. London Ser. A **324**, 301 (1971).
[42] D.M. Schaefer, M. Carpenter, B. Gady, R. Reifenberger, L.P. DeMejo, and D.S. Rimai, J. Adhes. Sci. Technol. (to be published).
[43] J. Belak, D.B. Boercker, and I.F. Stowers, MRS Bull. B **64**, 55 (1993).
[44] Charles Kittel, *Introduction to Solid State Physics*, 6th ed. (Wiley, New York, 1986).